www.ThePharmaJournal.com

The Pharma Innovation

ISSN (E): 2277- 7695
ISSN (P): 2349-8242
NAAS Rating: 5.23
TPI 2021; SP-10(12): 624-631

www.thepharmajournal.com
Received: 10-10-2021
Accepted: 16-11-2021

Gulshan Kumar
ICAR-Central Institute of Fisheries Education, Mumbai, Maharashtra, India

Gireesh-Babu P
ICAR-Central Institute of Fisheries Education, Mumbai, Maharashtra, India

KV Rajendran
ICAR-Central Institute of Fisheries Education, Mumbai, Maharashtra, India

Mukunda Goswami
ICAR-Central Institute of Fisheries Education, Mumbai, Maharashtra, India

Aparna Chaudhari
Head, Fish Genetics and Biotechnology Division, ICAR-Central Institute of Fisheries Education, Mumbai, Maharashtra, India

Corresponding Author
Aparna Chaudhari
Head, Fish Genetics and Biotechnology Division, ICAR-Central Institute of Fisheries Education, Mumbai, Maharashtra, India

Molecular dynamics of white spot syndrome virus envelope protein VP28 suggests a unique mechanism of membrane fusion

Gulshan Kumar, Gireesh-Babu P, KV Rajendran, Mukunda Goswami and Aparna Chaudhari

Abstract
White spot syndrome virus (WSSV) causes white spot disease in shrimp resulting in huge economic losses. WSSV is a large enveloped virus and a trimeric envelope protein VP28 mediates its entry into host cells. The crystal structure of VP28 is reported, but the conformational transitions leading to membrane fusion are unknown. Here, atomistic molecular dynamic (MD) simulation of VP28 without its transmembrane domain was performed in water at physiological pH. The trimer opened up and dissociated multiple times without major conformational changes in its β-barrel domain, and only the N-terminal α-helical region showed sideways movement. Each monomer had equal probability of separating with accompanied increase in solvent accessible surface area and loss of H-bonds. Free energy of dissociation values revealed that VP28 trimer is three times less stable than the structurally similar Class III baculovirus envelope glycoprotein gp64, and possibly adopts a unique fusion mechanism.

Keywords: White spot virus, computational analysis, envelope glycoprotein, virus entry

1. Introduction
White spot disease caused by White Spot Syndrome Virus (WSSV) is one of the most significant shrimp diseases causing high annual economic losses to the aquaculture industry. When it first broke out in Taiwan in 1992 it caused nearly complete mortality within 3 to 10 days, and spread rapidly to almost all the major shrimp farming countries including Asia, Middle East, North, Central and South America devastating *Penaeus monodon* culture prevalent at that time (Pradeep *et al*. 2012) [1]. Till today, no efficient antiviral therapeutic agent is available to control this disease and the preventive measures employed are of little consequence. The Asian shrimp industry adopted *Penaeus vannamei* as the culture species due to availability of specific pathogen free seed, but in countries where WSSV is endemic, even this species suffers losses during the culture period. WSSV is a double-stranded DNA virus of genus *Whispovirus* and family *Nimaviridae*, with a circular genome of approximately 300 kb in size. Number of putative ORFs varies from 515 to 684 among the isolates identified from different geographical regions (Verbruggen *et al*. 2016) [2].
WSSV virion is comparatively large in size and rod-shaped with dimensions in the range of 80-120 × 250-380 nm. It consists of a nucleocapsid surrounded by a trilaminar unit membrane envelope with a tail-like appendage (Escobedo-Bonilla *et al*. 2008) [3]. Its envelope contains structural proteins including the most common VP28 (Xie and Yang 2006) [4]. This glycoprotein is important for virus entry and pathogenesis (Dimitrov 2004; Plemper 2011) [5, 6]. Based on structural organization and fusion mechanism three distinct classes of viral envelope glycoproteins (EGs) are described, namely, Class I, II and III. All these undergo striking conformational changes and refolding to engage virus and host membranes. Some of the well-studied examples of envelope proteins mediating membrane fusion include influenza HA (Bullough *et al*. 1994; Plemeper 2011) [7, 6] and paramyxovirus F (Swanson *et al*. 2010; Plemepr 2011) [8, 6] of class I; flavovirus E (Sánchez-San Martín *et al*. 2009) [9] of class II; herpes virus gB (Backovic *et al*. 2009) [10] and baculovirus gp64 (Kadlec *et al*. 2008) [11] of Class III. Class I EGs that were the first to be crystallized are homo-trimeric and require a pH sensitive proteolytic cleavage to become active. The membrane fusion is either mediated by low pH only (e.g. influenza HA) or receptor binding in conjunction with low pH (e.g. paramyxovoruses F). Class II EGs are dimers that remain in elongated plate like structures parallel to the virus envelope. They contain a fusion loop that is initially buried in the dimer interface, but comes out towards the target membrane at low pH.

Class III EGs are homo-trimers like Class I, but each monomer has a fusion loop and membrane fusion or receptor binding is triggered by low pH. The baculovirus envelope protein gp64 that mediates membrane fusion with insect host cells is a Class III protein. Since WSSV also has invertebrate hosts, and VP28 has structural similarity with gp64, free energies of association and dissociation have been compared here to see whether VP28 behaves like Class III EGs.

WSSV VP28 gene, first identified by van Hulten *et al*. (2000) [12] cods for a 204 amino acid long peptide with a M.W. of ~28 kD. N-terminal region contains hydrophobic residues with a putative transmembrane α-helix formed by amino acids 9–27. The C-terminal region comprising of 28-204 residues is predicted to remain exposed outside the envelope and takes part in receptor binding. Residues 1-8 remain in tegument, the region between envelope and nucleocapsid (van Hulten *et al*. 2000) [12]. Yi *et al*. (2004) [13] showed the role of VP28 in virus internalization in primary culture of lymphoid organ of *Penaeus monodon*. With the help of EGFP reporter they showed that VP28 binds to the cell membrane and gets internalized. Further treatment of infected shrimps with polyclonal antibodies against VP28 delayed mortalities indicating its role in virus penetration (van Hulten *et al*. 2001) [14]. The antigenic property of this protein was confirmed by Du *et al*. (2013) [15]. They claimed more than 80% survival of crayfish injected with a mixture of WSSV and anti-VP28 polyclonal antibodies. Similarly, marine bioactive compounds against this protein were also identified by *in silico* approach (Sivakumar *et al*. 2016). RNA interference molecules targeting VP28 have been shown to be protective in different shrimp species (Xu *et al*. 2007; Krishnan *et al*. 2009; Zhu and Zhang 2012) [16, 17, 18].

Tang *et al*. (2007) [19] characterized the 3-D structure of WSSV VP28, by crystalizing it as a trimer without the transmembrane region. The truncated VP28 gene was expressed in *E. coli*, and each monomer was reported to have a β-barrel architecture with a protruding N-terminal helix. This N-terminal helix is attached to the β-core through a 2 amino acid coil. Nine β-strands (β1 – β9) are arranged mostly in an antiparallel fashion to form the β-barrel. One additional α-helix hangs outside the β-barrel. The β-barrel contains a central pore which is highly hydrophobic in nature. Analysis of purified WSSV by non-reducing SDS-PAGE, western blotting and MALDI-TOF MS showed trimeric, dimeric and monomeric conformations of VP28 in solution (Tang *et al*. 2007) [19]. Conformational dynamics of VP28 protein and its role in fusion of the virus with the host is still unknown.

Molecular dynamic (MD) simulation is a valuable tool that reveals atomic detail of structural dynamics of protein molecule. MD can reveal the stepwise mechanism of conformational change including subunit association and dissociation of a multimeric complex (Plattner *et al*. 2017; Karplus and Kuriyan 2005; Liu *et al*. 2013; Zhang *et al*. 2016; Hollingsworth and Dror 2018; Geng *et al*. 2019; Pan *et al*. 2019; Su and Wu 2019) [20, 21, 22, 23, 24, 25, 26, 27] and dissociation. It is not yet possible to observe such conformational transitions in real time in the lab. Techniques like X-ray crystallography and cryoelectron microscopy can only give static images of different conformational states of protein complexes. MD simulation studies are commonly done to observe functional processes such as ligand binding, ligand- or voltage-induced-conformational changes protein folding or membrane transport. There are several studies where MD simulation results could be validated by follow up experiments. Dror *et al*. (2015) [28] studied the structural mechanism of G-protein activation by GPCR using MD simulation, and the results could be validated by isothermal titration calorimetry, spectroscopy and mutagenesis (Dror *et al*. 2015; Hollingsworth and Dror 2018) [28, 24]. Similarly, Latorraca *et al*. (2017) [29] successfully captured the outward open, intermediate and inward open conformations of a sugar transporter using MD simulation that could be later confirmed by X-ray crystallography, mutagenesis and activity assay. MD simulation protocols are also used to explore the conformational space of peptides and small proteins. It can fold peptides even up to 80 amino acids to their native conformations (Geng *et al*. 2019) [25]. In present study 3-D structure and conformational flexibility of WSSV EG VP28 protein was analyzed and compared to some extent with baculovirus gp64 using computational tools in order to understand its mechanism of membrane fusion.

2. Materials and Methods

2.1 Structural retrieval and editing

Crystal structure of WSSV envelope protein VP28, PDB ID 2ED6 of resolution 2 Å was downloaded from PDB database. The structure was visualized and edited by UCSF-Chimera (Pettersen *et al*. 2004) [30]. The structure was available in the form of assembly of 4 units with each unit composed of a trimeric assembly. Individual trimer unit which is considered to be the commonly occurring state in the viral envelope was taken for further analysis. The available structure lacks 31 amino acids of N-terminal transmembrane segment. The crystal structure of baculovirus envelope protein gp64 (PDB ID 3DUZ) was also retrieved for comparison.

2.2 Prediction of free energy of dissociation and buried surface area

Free energies of dissociation (ΔG^{diss}) of WSSV VP28 and baculovirus gp64 without their transmembrane regions were predicted from PDBePISA server (Krissinel and Henrick 2007) [31] in kcal/M. The free energy of dissociation corresponds to the difference in free energy between dissociated and associated states. The parameter free energy per unit of buried surface (cal/M/Å^2) area is a measure of the stability of complexes (Day *et al*. 2012) [32]. This parameter was calculated by for VP28 and gp64.

2.3 Molecular dynamic simulation

VP28 structure retrieved in the above step was used for MD simulation to study conformational changes in the structure. The structure was simulated at physiological pH using CHARMM36 Nov 2018 force-field (Huang *et al*. 2017) [33] using GROMACS 2018.1 tool (Berendsen *et al*. 1995; Abraham *et al*. 2015) [34, 35]. The structure was solvated in water in a cubic box with protein placed at 1.0 nm distance from the box edges. Three point water model SPC216 was used for solvation. A total of 22116 water molecules were added with system size 6.156 6.587 6.625 nm and box volume 768.20 nm^3. To neutralize the system, 24 solvent molecules were replaced by 24 Na^+ ions in ion addition step. The system was energy minimized using steepest descent method to a maximum force 1000.0 KJ/mol/nm with step size 0.01 and 50000 steps. Long-range electrostatics was treated using Particle Mesh Ewald (PME) method. The system was first NVT equilibrated for 100 ps with time step 2 fs using modified Berendsen thermostat. The system is again equilibrated for pressure stabilization by using NPT

equilibration step for 100 ps with time step 2 fs using Parrinello-Rahman isotropic pressure coupling. After equilibrations, system was taken for production MD for 50 ns simulation time with a time step 2 fs using leap-frog integrator. Long-range electrostatics was treated again using PME method. MD run was conducted with both temperature and pressure coupling on.

2.4 MD data analysis and structural comparison

Various graphs were plotted using XMGRACE 5.1.19 (Turner, 2005) [36] graph plotting tool. MD movie making, structural comparison and other analysis were conducted using UCSF-Chimera 1.13.1 software package.

Matchmaker tool of UCSF-Chimera (Pettersen *et al*. 2004) [30] software was used for superimposition of structures. VP28 structures at the beginning of MD and before dissociation events were superimposed to see structural changes that occurred before dissociation of monomers. The alignment algorithm used was Needleman-Wunsch with BLOSUM-62 matrix. Matching was iterated by pruning long atom pairs until no atom pairs exceeded 2.0 Å.

2.5 Interaction analysis among monomers

The total number of hydrogen bonds between separating chain A monomer and BC dimer as a function of time were calculated using gmx hbond command. The criteria for the formation of H-bond were 3.5 Å cutoff distance between donor-acceptor atoms and 30° cutoff angle formed by hydrogen-donor-acceptor.

2.6. Calculation of solvent assessable surface area

Solvent assessable surface area (SASA) as a function of time was calculated using gmx sasa command using a solvent probe of radius 1.4 Å.

3. Results

3.1 Free energy of dissociation

ΔG^{diss} of VP28 and gp64 (PDB ID (3DUZ) were 25.5 kcal/mol and 319.0 kcal/mol, respectively. Buried surface areas for VP28 and gp64 were 20510 $Å^2$ and 32080 $Å^2$, respectively. ΔG^{diss} dissociation per unit buried surface area for VP28 and gp64 were 9.9 cal/mol/$Å^2$ and 3.77 cal/mol/$Å^2$ respectively. This indicates the higher stability of the gp64 trimer in solution.

3.2 MD simulation

The structure was energy minimized by steepest descent method for 389 ps. The initial potential energy was -5.589 $\times 10^5$ kJ/mol and after 389 ps, it got a value around -1.198 $\times 10^6$ kJ/mol. This was the final value obtained at the plateau of the potential energy curve. Similarly, during temperature and pressure equilibration, the system's temperature remained close to 300 K and density remained around 1035 kg/m^3 revealing the stability of the system. Root mean square deviation (RMSD) of the backbone of protein was analyzed with respect to initial structure to know the overall change in the structure.

The complex remained stable throughout the simulation with RMSD value around 0.2 nm except at the time of separation. During separation events RMSD attained a value around 3.6 nm (Fig.1). The value remained unchanged throughout rest of the simulation period except at the time separation of monomers. For the measurement of compactness of protein structure, radius of gyration (Rg) was observed throughout the simulation. Rg value was fluctuated around 2.3 nm throughout the simulation but at the separation events it went up to 4.5 nm (Fig.2).

Systems trajectory was visualized in the form of MD movie where the whole simulation was divided in 5000 frames. During movie visualization and trajectory analysis total three separation events were encountered at 9th ns (starting frame 0912), 34th ns (starting frame 3454) and third separation event at 36th ns (starting frame 3631). First and second separation events were composed of multiple closely occurring separation events. First separation event was started at 9.12th ns and ended at 9.42th ns when chain A separated multiple times. Second separation event was started at 34.54th ns and ended at 34.66th ns when chain C separated multiple times. Third separation occurred at 36.31th ns when again chain A separated. These separation events can be easily seen in the bumps of RMSD and Rg curves. Root mean square fluctuation (RMSF) of the amino acid residues is a measure of deviation of a residue position with respect to its time averaged position throughout the simulation. It tells about the mobility of the structural regions and residues. RMSF value was obtained in the range of 0.15 nm to 0.6 nm, showing some regions with significantly greater mobility than others. In all three chains, N-terminal helix and hinge region were the most mobile regions (Fig. 3).

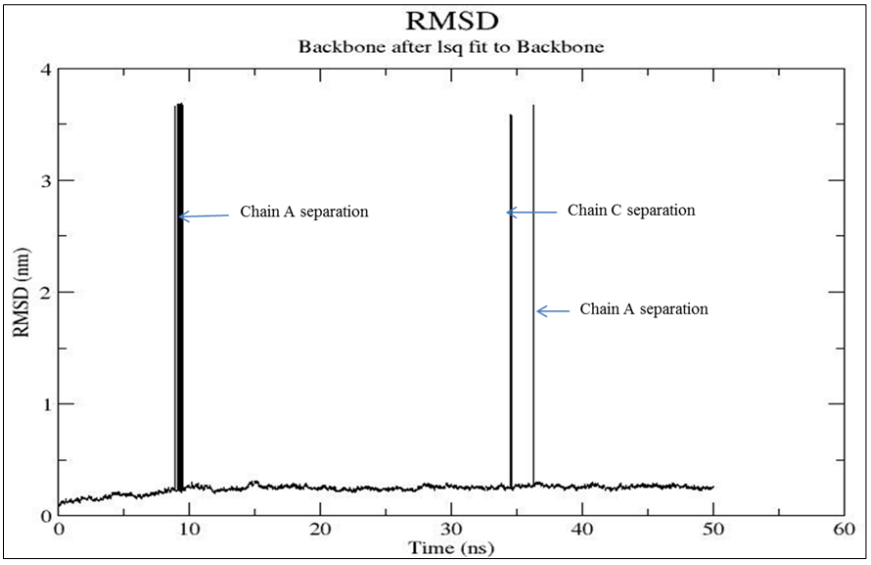

Fig 1: RMSD plot of VP28 trimer showing multiple separation events. Individual separation events have been marked

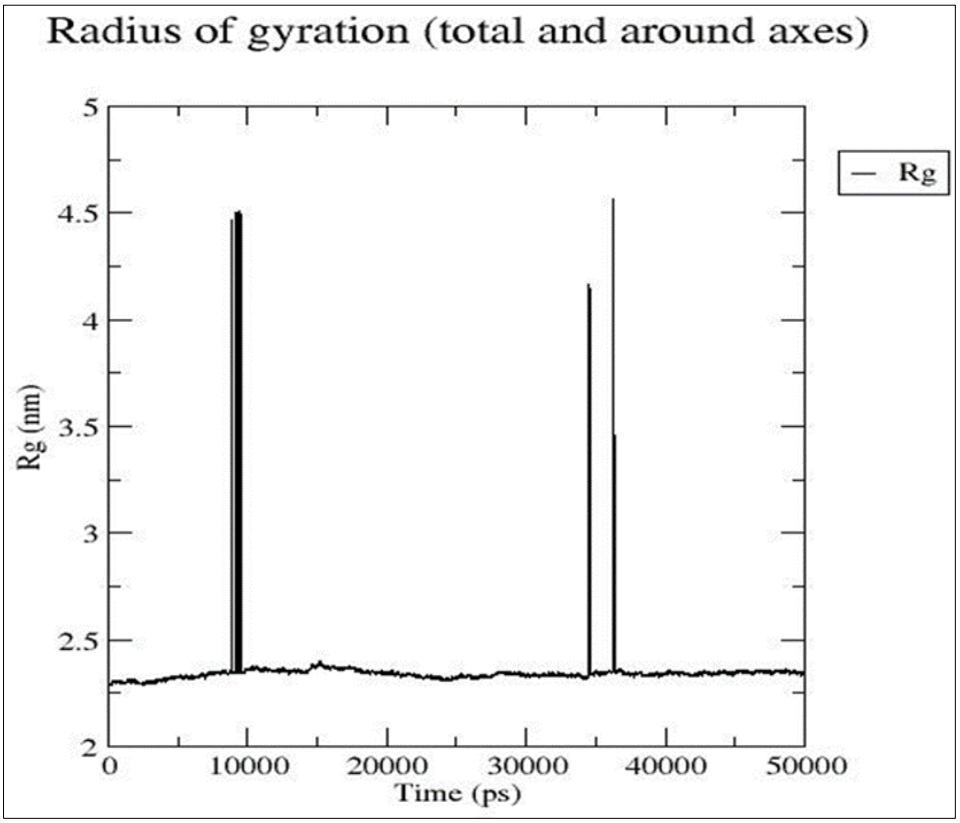

Fig 2: Radius of gyration (Rg) of VP28 trimer

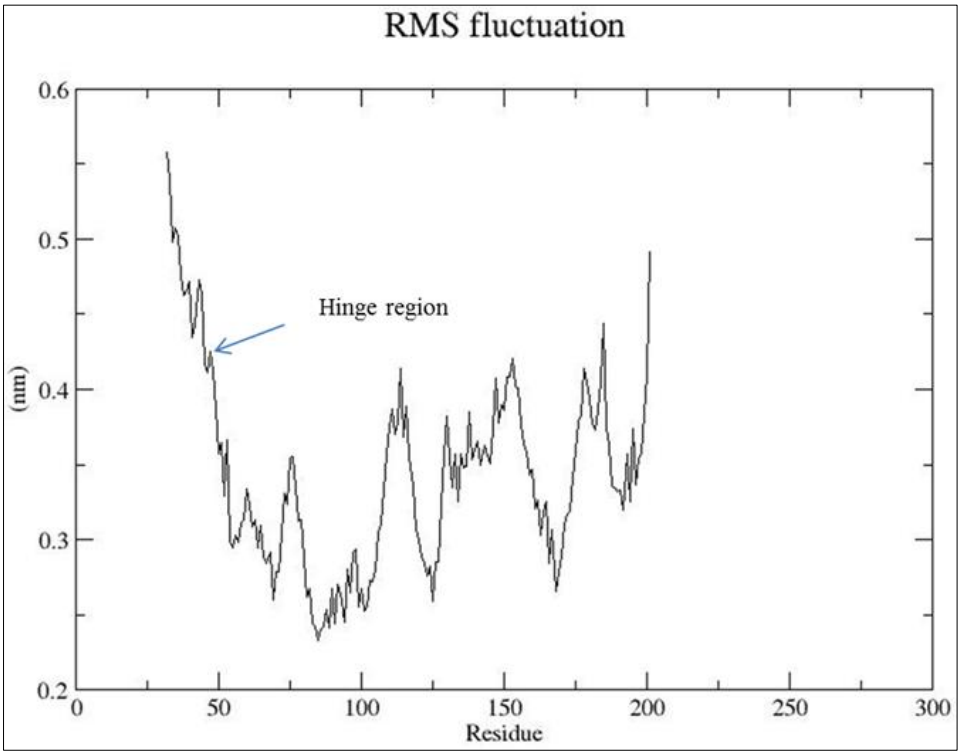

Fig 3: Residue wise RMSF plot of chain A of VP28 trimer. Hinge residue connecting N-terminal helix to β-barrel is marked

3.3 Structural comparison

Several structures obtained at nearly equal time interval were compared before the first separation event. These structures did not show any major conformational change in their β-barrel domain before separation (Fig. 4). There were movement in N-terminal helix and loops of β-barrel. Immediately before separation structure opened up and dissociated.

As simulation proceeded, the N-terminal helix changed conformation and deviated significantly as compared to the core β-barrel. N-terminal helices of all the three subunits shifted aside as simulation proceeded (Fig. 5).

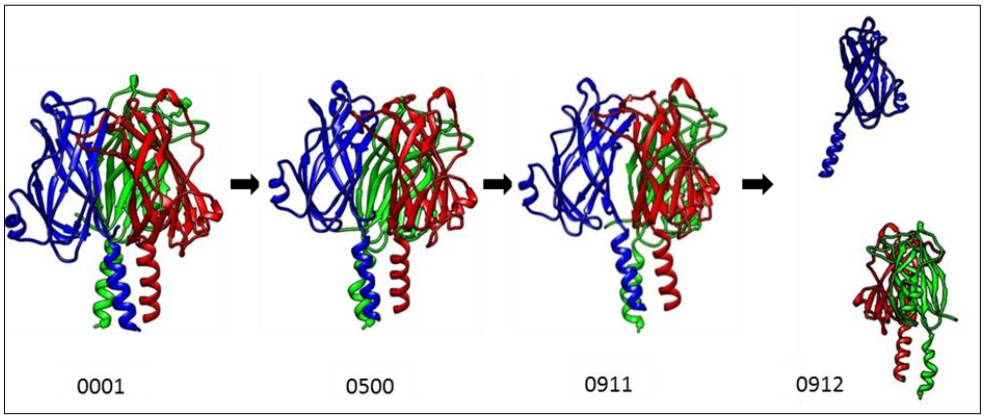

Fig 4: Conformational transitions in VP28 trimer leading to first separation event when chain A separates at 9th ns (frame no. 0912). Images have been arranged according to frame number which is written below each image. Chain A, B and C is colored as blue, green and red respectively

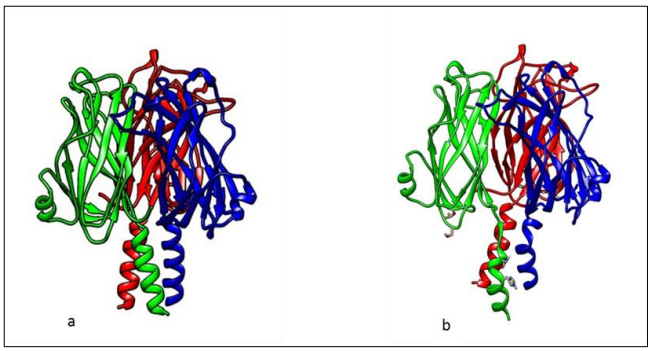

Fig 5: Conformational changes in N-terminal helix of VP28 trimer is shown. a. image of trimer at 1st ns and b. image of trimer at 36th ns.

3.4 Interaction analysis

Interaction among the monomers was analyzed to see changes in the number and pattern of H-bonding in the fluctuating structure. Total number of H-bonds formed by separating chain A with its partner dimer BC was 12 in the beginning of simulation. At 1.36th ns the number reached its maximum value of 15. Similarly, at beginning of the 4th ns it was close to its maximum value. The number started declining from the beginning of the 5th ns and decreased until the separation event at 9th ns when the minimum value of 3 was reached (Fig. 6).

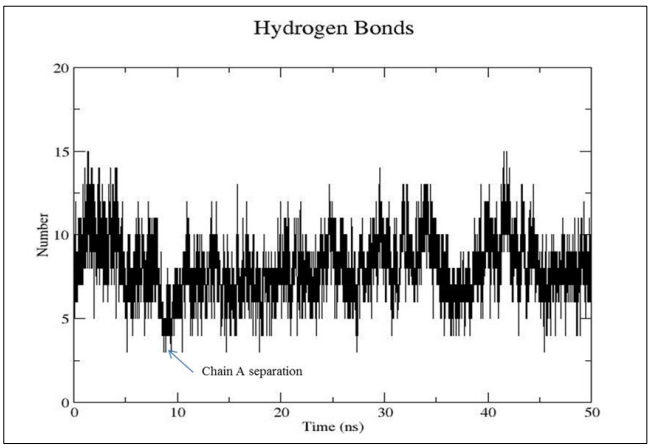

Fig 6: Number of H-bonds formed by chain A with B and C plotted with respect to time. First separation event of chain A has been marked

3.5 Solvent assessable surface area

At the beginning of simulation, SASA of separating chain A was 92.8 nm^2. It started to increase till the time of separation. It attained its maximum value of 101 nm^2 at the beginning of the 8th ns and remained ~100 nm^2 during the separation (Fig. 7). A 7-8% gain in SASA was observed in each monomer during the separation event.

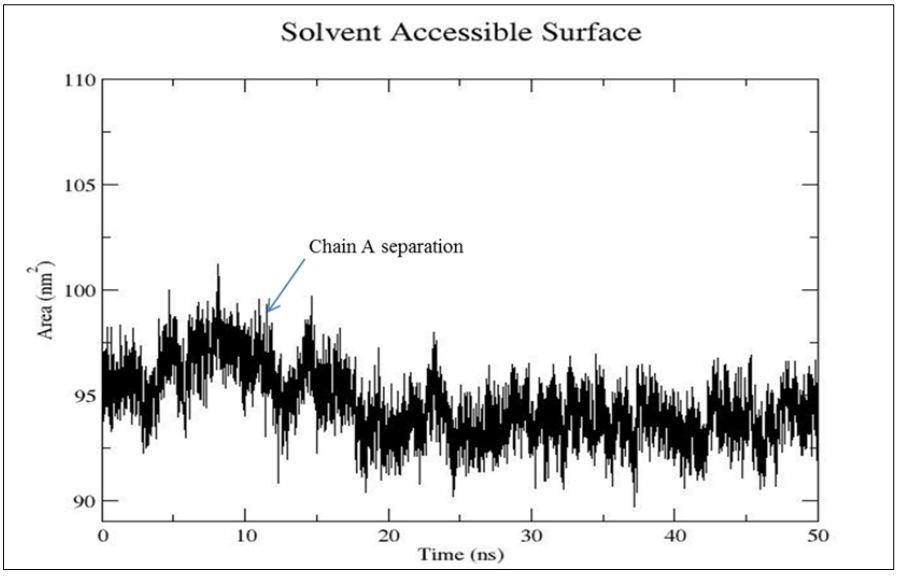

Fig 7: Solvent assessable surface area of chain A is plotted with respect to time. First separation event of chain A has been marked

4. Discussion

Infection of a host cell by an enveloped virus requires fusion of the viral envelope and the host cell membrane. This process transfers viral genetic material into the host cell. The fusion of lipid membranes is an energy dependent process due to repulsion between the approaching membranes. Viral envelope proteins carry out this process by engaging key membrane proteins of the host (Plemper 2011) [6]. Depending on the structural organization and fusion mechanism, three distinct classes of viral envelope proteins are described namely class I, II and III.

WSSV was earlier classified as a member of *baculoviridae* family (van Hulten *et al*. 2001; Mayo 2002) [14, 37] and the overall shape of its envelope protein VP28 also looks quite similar to class III envelope proteins like the baculovirus envelope protein gp64 that is well characterized (Kadlec *et al*. 2008; Plemper 2011) [11, 6]. Class III envelope proteins are trimeric in pre- and post-fusion conformations and their shape resembles a tripod. They undergo three conformational shifts to carry out membrane fusion namely native pre-fusion conformation, an extended conformation engaging both virus and host membrane and a hairpin like post-fusion conformation. These proteins contain a fusion loop associated with each leg of tripod pointing towards viral envelope in pre-fusion conformation. Fusion event is triggered by low pH inducing swinging of tripod leg towards target membrane. Domain II of baculovirus gp64 contains a fusion peptide composed of three antiparallel β-sheets and one small α-helix rich in hydrophobic and charged residues. Each monomer contributes 3 His residues to form a 9 His cluster present at the oligomerisation interface. This cluster works as a pH sensor and enables conformational change for membrane fusion at low pH. Due to the presence of disulfide bridges and high binding energy per unit of buried surface area this molecule is expected to remain trimeric during the entire fusion event.

WSSV is transported to early endosomes through endocytosis process. During maturation endosomes get acidified and membrane fusion or lysis of the endosomal compartment is triggered leading to viral escape (Verbruggen *et al*. 2016) [2]. A region between the residues 70-102 of VP28 looks similar to gp64 fusion peptide. This region is composed of three antiparallel β-strands and a small helix, and contains hydrophobic and charged residues. Each monomer contributes two His residues, His 40 and His 195, to the interface of oligomerization. These residues could serve as pH sensors during low pH to trigger membrane fusion. This could be further confimred using mutagenesis techniques. With only 6 His residues at the interface instead of 9 present in gp64, and due to the absence of disulfide bridges, the VP28 trimer is less stable. The required dissociation energy per unit of buried surface calculated for gp64 in the study is almost three times higher than VP28. In MD analysis too the VP28 trimer dissociates easily. This indicates that the mechanism of membrane fusion adopted by WSSV is different from that of Class III GPs and could fall in a class of its own, even though there is much similarity with gp64 in terms of overall structure.

This study revealed that in an all-atom 50 ns MD simulation in water the VP28 trimer dissociated to its monomers and then re-associated multiple times without major intra-subunit conformational change. Conformational changes were observed only in the N-terminal α-helices, which can be considered analogous to baculovirus gp64 tripod legs. The helix bundle moved sideways and tilted. This movement in tripod leg was mediated by the flexible hinge loop connecting the legs to globular β-barrel domain.

Tang *et al*. (2007) [19] reported the crystal structure of WSSV VP28 and VP26 (a nucleocapsid/ tegument protein) trimers without the trans membrane domain, Based on wet-lab studies, Tang *et al*. (2007) [19] proposed that VP28 and VP26 exist as trimers in the viral envelope, like the baculovirus gp64, but the monomeric state was most abundant in solution, as the subunits are not bonded by covalent bonds but weak interactions. It has been suggested that the presence of multi-conformational states (monomer, dimer and trimer) in solution could enable this protein to perform more than one role (Tang *et al*. 2007; Sun *et al*. 2016) [19]. Similarly, the crystal structure of another nucleocapsid protein of WSSV VP24 was determined by Sun *et al*. (2016) [38]. The crystal symmetry revealed a trimeric state, but in solution the monomer was most prominent. It was proposed that monomeric-trimeric transition may be essential during WSSV pathogenesis. In this study, a total three separation events were seen during 50 ns MD simulation of VP28 crystal structure in solution confirming the dissociation of trimeric VP28. This is in accordance with the results of Tang *et al*. (2007) [19] and Sun *et al*. (2016) [38]. Chain A of trimer got separated two times and chain C one time from the trimer revealing equal chances of separation of all the three chains. This can also be inferred from the binding free energy of all three subunits as well as crystal symmetry.

In MD studies the mechanism of dissociation can be studied in great detail, which is not possible with existing laboratory techniques. There are several reports where MD was applied to study association-dissociation events of oligomeric proteins. Pan *et al*. (2019) [26] studied association-dissociation events of six structurally and functionally different dimeric proteins, which do not undergo conformation change after binding. They applied long-time scale all atom molecular dynamics with an enhanced sampling approach as well as conventional all atom dynamics for their study. The separated monomers from five dimers get associated to form the native conformation after passing through non-native states, thus proving the validity of the method. Zhang *et al*. (2016) [23] performed unstrained all atom MD to study dissociation dynamics of heterodimer SAM domains of Eph2 and SHIP2 molecules, and observed subtle conformation changes including domain rotation and pivoting, translation and simultaneous rolling to attenuate and weaken binding interfaces.

Here it is seen that dissociation of VP28 does not involve any major conformational change before dissociation. This was the case for all the separation events sampled throughout the simulation. The region of the β-barrel that interacts with the other two subunits does not show any significant conformational change before dissociation, and only the N-terminal α-helical region shows sidewise movement. The subunits did not explore non-native binding interfaces on the protein surface before separation but proceeded by losing H-bonds. The number of H-bonds became less than half before separation. Dissociation was accompanied by a steady increase in the solvent accessible surface area as in other cases (Zhang *et al*. 2016; Pan *et al*. 2019) [23, 26].

5. Conclusion

The present study concludes that it is very likely that the dissociation of the key WSSV envelope glycoprotein VP28

happens without any major conformational change in its core structure. In spite of structural similarities with the baculovirus gp64, WSSV VP28 does not behave like Class III envelope glycoproteins, but adopts a peculiar mechanism for viral entry.

6. Acknowledgement

The authors would like to acknowledge ICAR for providing fellowship to the first author and Director, ICAR-Central Institute of Fisheries Education, Mumbai for providing the necessary facilities to carry out this research.

7. References

1. Pradeep B, Rai P, Mohan SA, Shekhar MS, Karunasagar I. Biology, host range, pathogenesis and diagnosis of white spot syndrome virus. Indian Journal of Virology 2012;23(2):161-74.
2. Verbruggen B, Bickley LK, Van Aerle R, Bateman KS, Stentiford GD, Santos EM *et al*. Molecular mechanisms of white spot syndrome virus infection and perspectives on treatments. Viruses 2016;8(1):23.
3. Escobedo-Bonilla CM, Alday-Sanz V, Wille M, Sorgeloos P, Pensaert MB, Nauwynck HJ. A review on the morphology, molecular characterization, morphogenesis and pathogenesis of white spot syndrome virus. Journal of fish diseases 2008;31(1):1-8.
4. Xie X, Yang F. White spot syndrome virus VP24 interacts with VP28 and is involved in virus infection. Journal of General Virology 2006;87(7):1903-8.
5. Dimitrov DS. Virus entry: molecular mechanisms and biomedical applications. Nature Reviews Microbiology 2004;2(2):109-22.
6. Plemper RK. Cell entry of enveloped viruses. Current opinion in virology 2011;1(2):92-100.
7. Bullough PA, Hughson FM, Skehel JJ, Wiley DC. Structure of influenza haemagglutinin at the pH of membrane fusion. Nature 1994;371(6492):37-43.
8. Swanson K, Wen X, Leser GP, Paterson RG, Lamb RA, Jardetzky TS. Structure of the Newcastle disease virus F protein in the post-fusion conformation. Virology 2010;402(2):372-9.
9. Sánchez-San Martín C, Liu CY, Kielian M. Dealing with low pH: entry and exit of alphaviruses and flaviviruses. Trends in microbiology 2009;17(11):514-21.
10. Backovic M, Longnecker R, Jardetzky TS. Structure of a trimeric variant of the Epstein–Barr virus glycoprotein B. Proceedings of the National Academy of Sciences 2009;106(8):2880-5.
11. Kadlec J, Loureiro S, Abrescia NG, Stuart DI, Jones IM. The postfusion structure of baculovirus gp64 supports a unified view of viral fusion machines. Nature structural & molecular biology 2008;15(10):1024-30.
12. Van Hulten MC, Westenberg M, Goodall SD, Vlak JM. Identification of two major virion protein genes of white spot syndrome virus of shrimp. Virology 2000;266(2):227-36.
13. Yi G, Wang Z, Qi Y, Yao L, Qian J, Hu L. Vp28 of shrimp white spot syndrome virus is involved in the attachment and penetration into shrimp cells. BMB Reports 2004;37(6):726-34.
14. Van Hulten MC, Witteveldt J, Peters S, Kloosterboer N, Tarchini R, Fiers M *et al*. The white spot syndrome virus DNA genome sequence. Virology 2001;286(1):7-22.
15. Du HH, Hou CL, Wu XG, Xie RH, Wang YZ. Antigenic and immunogenic properties of truncated VP28 protein of white spot syndrome virus in *Procambarus clarkii*. Fish & shellfish immunology 2013;34(1):332-8.
16. Xu J, Han F, Zhang X. Silencing shrimp white spot syndrome virus (WSSV) genes by siRNA. Antiviral research 2007;73(2):126-31.
17. Krishnan P, Babu PG, Saravanan S, Rajendran KV, Chaudhari A. DNA constructs expressing long-hairpin RNA (lhRNA) protect *Penaeus monodon* against White Spot Syndrome Virus. Vaccine 2009;27(29):3849-55.
18. Zhu F, Zhang X. Protection of shrimp against white spot syndrome virus (WSSV) with β-1, 3-D-glucan-encapsulated vp28-siRNA particles. Marine biotechnology 2012;14(1):63-8.
19. Tang X, Wu J, Sivaraman J, Hew CL. Crystal structures of major envelope proteins VP26 and VP28 from white spot syndrome virus shed light on their evolutionary relationship. Journal of virology 2007;81(12):6709-17.
20. Plattner N, Doerr S, De Fabritiis G, Noé F. Complete protein–protein association kinetics in atomic detail revealed by molecular dynamics simulations and Markov modelling. Nature chemistry 2017;9(10):1005-11.
21. Karplus M, Kuriyan J. Molecular dynamics and protein function. Proceedings of the National Academy of Sciences 2005;102(19):6679-85.
22. Liu FF, Huang B, Dong XY, Sun Y. Molecular basis for the dissociation dynamics of protein A-immunoglobulin G1 complex. PLoS One 2013;8(6):e66935.
23. Zhang L, Borthakur S, Buck M. Dissociation of a dynamic protein complex studied by all-atom molecular simulations. Biophysical journal 2016;110(4):877-86.
24. Hollingsworth SA, Dror RO. Molecular dynamics simulation for all. Neuron 2018;99(6):1129-43.
25. Geng H, Chen F, Ye J, Jiang F. Applications of molecular dynamics simulation in structure prediction of peptides and proteins. Computational and structural biotechnology journal 2019;17:1162-70.
26. Pan AC, Jacobson D, Yatsenko K, Sritharan D, Weinreich TM, Shaw DE. Atomic-level characterization of protein–protein association. Proceedings of the National Academy of Sciences 2019; 116(10):4244-9.
27. Su Z, Wu Y. Computational studies of protein–protein dissociation by statistical potential and coarse-grained simulations: A case study on interactions between colicin E9 endonuclease and immunity proteins. Physical Chemistry Chemical Physics 2019;21(5):2463-71.
28. Dror RO, Mildorf TJ, Hilger D, Manglik A, Borhani DW, Arlow DH *et al.* Structural basis for nucleotide exchange in heterotrimeric G proteins. Science 2015;348(6241):1361-5.
29. Latorraca NR, Fastman NM, Venkatakrishnan AJ, Frommer WB, Dror RO, Feng L. Mechanism of substrate translocation in an alternating access transporter. Cell 2017;169(1):96-107.
30. Pettersen EF, Goddard TD, Huang CC, Couch GS, Greenblatt DM, Meng EC *et al*. UCSF Chimera—a visualization system for exploratory research and analysis. Journal of computational chemistry 2004;25(13):1605-12.
31. Krissinel E, Henrick K. Inference of macromolecular assemblies from crystalline state. Journal of molecular biology 2007;372(3):774-97.
32. Day ES, Cote SM, Whitty A. Binding efficiency of protein–protein complexes. Biochemistry

2012;51(45):9124-36.
33. Huang J, Rauscher S, Nawrocki G, Ran T, Feig M, De Groot BL *et al*. CHARMM36m: an improved force field for folded and intrinsically disordered proteins. Nature methods 2017;14(1):71-3.
34. Berendsen HJ, Van der Spoel D, van Drunen R. GROMACS: a message-passing parallel molecular dynamics implementation. Computer physics communications 1995;91(1-3):43-56.
35. Abraham MJ, Murtola T, Schulz R, Páll S, Smith JC, Hess B *et al*. GROMACS: High performance molecular simulations through multi-level parallelism from laptops to supercomputers. Software X 2015;1:19-25.
36. Turner PJ. XMGRACE, Version 5.1. 19. Center for Coastal and Land-Margin Research, Oregon Graduate Institute of Science and Technology, Beaverton, OR 2005.
37. Mayo M. A summary of taxonomic changes recently approved by ICTV. Archives of virology 2002;147(8):1655-6.
38. Sun L, Su Y, Zhao Y, Fu ZQ, Wu Y. Crystal structure of major envelope protein VP24 from white spot syndrome virus. Scientific reports 2016;6(1):1-9.